Scilight

Thermal Science and Applications
https://www.sciltp.com/journals/tsa

Article

Transient Gas to Gas Experimental Study in a Bitubular Configuration Heat Exchanger

Michel Feidt [1] and Monica Costea [2,*]

[1] Laboratory of Energetics, Theoretical and Applied Mechanics (LEMTA), URA CNRS 7563, University of Lorraine, 54518 Vandoeuvre-lès-Nancy, France
[2] Department of Engineering Thermodynamics, National University of Science and Technology POLITEHNICA Bucharest, Splaiul Independentei 313, 060042 Bucharest, Romania
* Correspondence: monica.costea@upb.ro

How To Cite: Feidt, M.; Costea, M. Transient Gas to Gas Experimental Study in a Bitubular Configuration Heat Exchanger. *Thermal Science and Applications* **2026**, *1*(2), 101–121. https://doi.org/10.53941/tsa.2026.100008

Received: 12 December 2025
Revised: 5 March 2026
Accepted: 1 April 2026
Published: 17 April 2026

Abstract: This paper presents a comprehensive experimental study of gas-gas flows inside a bitubular (shell-and-tube) heat exchanger (HEX) subjected to various transient conditions, namely (1) increasing or decreasing the internal hot fluid temperature, (2) increasing or decreasing the mass flow rate of the external cold fluid by step variation. Surprisingly, there are very few results in the literature for this last case. However, it seems to be of fundamental interest for some applications. Two types of quantity, the temperatures of the fluids and the heat fluxes exchanged in the HEX, are subject to transient conditions, with a range of time constants from 20 to 80 s. A comparison of experimental results with the main existing analytical model proposed in the literature, essentially validated with liquid-liquid flows, is performed. Deviations from analytical models are given as uncertainties of the time constants. It is shown that one temperature time constant is not suitable for the gas-gas flows. Extension of the results to the heat fluxes responses of the HEX is also performed and confirms the observed results. A sensitivity analysis of the time constants to the main system parameters is reported. It allows the identification of the most important influences and the proposal of primary explanations for the observed results. Local experiments on the same HEX configurations are under development, as well as associated analytical and numerical models. However, the aim is to preserve the simplicity and robustness of the models, to successfully apply them to (real time) control and command of any type of HEX using the equivalent bitubular model. This practical implication, together with the main conclusions of the sensitivity analysis of time constants provides useful insights for modelling and control applications.

Keywords: bitubular heat exchanger; transient state; time constant; experimental study; gas-gas

1. Introduction

Heat exchangers (HEX) are essential components of thermal systems and processes, as well as for transport applications. Compactness is the dominant characteristic to minimize the weight of the HEX and to control and command their transient behavior.

Transient conditions are natural in solar systems due to daily, seasonal, and meteorological variations [1,2]. The non-stationary regime is also fundamental to aerospace systems [3], such as launchers.

More frequently, physical discontinuities, such as the opening or closing of valve are common operations, for example in refrigerating and air conditioning systems. These types of transient conditions have been examined

and synthesized in a French research program [4]. The present bibliography could also include the transient behavior of automotive systems [5], developed especially nowadays, and more specifically with natural refrigerants such as CO_2 [6].

This first illustration of applications is closely related to research topics considered in our research group. But the interest in transient operation in HEX remains an important task today. The short list of published papers [7,8] confirms this fact and the need to consider the interaction of HEX with the system or process that includes it, such as data center [9,10], geothermal borehole [11] frost formation [12], magnetic refrigeration [13], thermoacoustic engine [14].

We will focus here on the HEX considered as the studied system, as illustrated by Ataer [15], who reports on the transient behavior of a finned-tube-cross flow HEX, subjected to a step variation of the hot fluid temperature. This liquid-gas HEX provides a corresponding temperature response for each fluid characterized analytically by the following three parameters: a time constant, a time lag, and a gain factor. The results have been compared favorably with both numerical calculations and experimental results. This paper illustrates that the most common studies are related to HEX without phase change, and, more specifically, to liquid-liquid HEX.

We note that modeling gas-gas systems is fundamentally different from modeling liquid-liquid HEX or two-phase flow HEX. We consider that dimensionless appraisal could intervene by summing up the modeling of these three categories. However, for many practical applications, the gas-gas system is preferred due to its characteristics, such as low thermal inertia, and compressibility effects.

Nevertheless, the great majority of papers consider specific cases, as follows:

- compact HEX [16]
- parallel- and counter-flow HEX [17]
- cross flow HEX with zero core capacitance [18]
- plate fin and tube HEX [19]
- airside heat transfer in cross flow HEX [20]
- cross flow HEX under variable temperature and flow rate conditions [21,22]
- plate HEX: influence of temperature disturbances and flow configurations [23].

We propose hereafter to classify the corresponding works into two categories, depending on:

A. Various kinds of imposed transient conditions in HEX

These conditions can be applied to counter-flow HEX configuration [24], which is the most favorable thermal situation, or to parallel-flow configuration [25].

It is also known that, regardless of the HEX studied, an equivalent bitubular HEX could be considered having the same characteristics [26]. This allows us to choose the bitubular HEX configuration as the reference for the proposed experiments, due to the generality of the results.

Among the transient conditions that can be imposed we mention:

(i) Temperature step: it has been particularly studied by J. Padet and his collaborators, references [27,28] reporting the experiments on bitubular HEX configuration for water-water flows, with inlet temperature step for one of the fluids (temperatures lower than 80 °C). The same study has been extended to simultaneous inlet temperatures disturbance [28,29].

For all these experiments, the exit temperature of the fluid T_{is} (internal or external) is modeled according to:

$$\begin{cases} T_{is}(t) = {T_{is}}^{o} \text{ if } t \le t_o \\ T_{is}(t) = {T_{is}}^{\infty} + ({T_{is}}^{o} - {T_{is}}^{\infty})\exp\left(-\dfrac{t - t_r}{\tau}\right) \; if \; t > t_o \end{cases} \quad (1)$$

This model is a two-parameters one (first order response), namely:

t_r, time lag,

τ, time constant.

(ii) Mass flow rate step: similar experiments have been done on bitubular HEX with mass flow rate step [30,31]. These studies have been completed by Abdelghani–Idrissi et al. [32,33] for a counter-flow bitubular HEX, where the corresponding mass flow rate step is applied on the internal hot fluid flow. This approach considers the longitudinal variation of the hot fluid time constant and gives the corresponding analytical formula. Note that these time constants are expressed only with data corresponding to the initial and final stationary states. The influence of the intensity of the increase (or decrease) of the mass flow rate on the temperatures is reported. The results are relative to liquids subjected to small perturbations inside the adiabatic HEX. Also, the time lag does not appear in this study.

(iii) Heat flux step: this type of step seems to be the most important for solar systems [34].

From a more fundamental point of view, ref. [35] presents a numerical analysis of the temperature profile in a rectangular channel subjected to a time varying heat flux. The fluid flows through the channel under laminar or turbulent conditions but is supposed iso-volume.

(iv) Other cases can be studied. To illustrate them, we briefly examine a paper [36] that proposes a theoretical study of one-dimensional heat transfer through a plate subjected to step variations of heat transfer coefficients on each side. The hot and cold fluids are supposed iso-volume and counter-flow configuration is used. This case study could be interesting for developing knowledge about the effects of thermal conduction inside the HEX walls. This will not be done here, and the corresponding results are currently considered as a guide for the proposed gas-gas experiments.

Regarding the solicitations (imposed constraints by the system), they can be summarized as:

- transient changes in flow [37]
- step changes in flow rates [38,39]
- perturbations in temperature and flow [21,22,40,41].

To conclude, many other references are provided in [42], as well as for measurement technics.

B. Transient measurements in HEX

Transient measurements technics are used for many years to estimate heat transfer coefficients [43].

Impulse method: this method has been used to determine the heat transfer coefficient between a fluid and a wall [44]. However, some precautions should be considered [45]. The reported case study is that of a uniformly heated plate with air flowing in front of it. The experiment consists of generating a disturbance of a stable convective regime by an energy pulse and observing the relaxation after the pulse. In reference [45], a comparison is made between the estimation of the heat transfer coefficient supposed to be constant, with the estimation that considers the variation of this coefficient over time, the second method being declared preferable.

The oscillatory method was developed in reference [43].

The single blow transient method uses only one fluid flow [46]. Due to that specificity, the heat transfer in question is relative to the flowing fluid and the wall in contact with the fluid. The system equations are solved by Laplace transform and numerical methods associated with inverse transform.

This method has been extensively used to determine heat transfer coefficients in compact HEX, where lateral conduction in the fins and axial conduction in the separation wall are important, as well as thermal dispersion in fluid.

To conclude this section, transient temperature or flow rates perturbation methods are common, as observed in the cited references (impulse, oscillatory change, step). Any change in inlet temperature has also been used [19] to determine the global heat transfer coefficient of a bitubular HEX. The method adopted in the present study complies with the proposal of J. Padet and his research group, mainly because it uses only step perturbations (temperature or mass flow rates) corresponding to the most important application cases. This robust method only requires knowledge of stationary states before ($t = 0$) and after ($t \to \infty$) the perturbation. It is known that in these cases, accurate correlations between heat and mass transfer are available in the literature.

The chosen HEX is the bitubular one, as this configuration allows the use of the results obtained through the equivalent HEX rule proposed in [26]. It also makes it possible to easily experience parallel-flow and counter-flow, for the entrance temperature or flow rate steps.

In fact, any heat exchanger could be characterized by an equivalent gas-gas bitubular configuration, also known as lumped system. The main assumptions of the system are related to entrance and exit distribution. Variation of the specific heat at constant pressure and constant volume is generally neglected. The exit distribution can be associated with fouling, which is assumed to be significant only in the long term.

The need for a first or second order model will be considered in the experiments, as well as the adaptation of the model to analyze not only temperature response but also heat rate response [26]. It seems that the temperature-heat rate duality response is not sufficiently considered in literature.

Last, but not least, it appears that very few results are relative to gas-gas flows in HEX. This configuration was chosen for our experiments, as the corresponding results could be useful for recuperators and other devices. It was tested for a temperature range from −80 °C to +250 °C, with a kinetics of 20 °C/s and for variable air properties (pressure and temperature).

The model included a bi-exponential function for the exit temperature of the perturbed fluid, to account for the low thermal inertia of the gas compared to that of the liquid.

An important and new result provided by the experiments is that the time constants corresponding to a step perturbation of temperature are different for the internal (perturbed) and external fluid (51.3 s ≠ 70.9 s). Then, another finding is related to the variation of the mass flow rates of the two fluids, which has a considerable influence on the values of the time constants and heat rate constant, i.e., the increase in the mass flow rate of the internal fluid $\dot{m}_{int}$ causes the decrease of the two time constants τ_{int} and τ_{Pint}.

The results provided by the transient regime of heat rates (less studied than that of temperature) and sensitivity analysis of the time constants to the main parameters of the system brought other information detailed in Section 3 and 4, useful for the control-oriented modeling of HEX.

2. Experimental Setup

2.1. Tested Coaxial HEX

Concentric HEX was chosen as the basic (reference) one. It allows parallel—and counter-flow study. Similitude rule has been proposed for transient conditions, that enables the results extension to any HEX configuration [26].

Heat Exchanger

Figure 1 illustrates a scheme of the tested coaxial HEX made of copper. Internal tube diameters are 20/22 mm and external tube diameters are 40/42 mm. Thermal insulation is placed on the external part of the HEX leading to negligible heat loss.

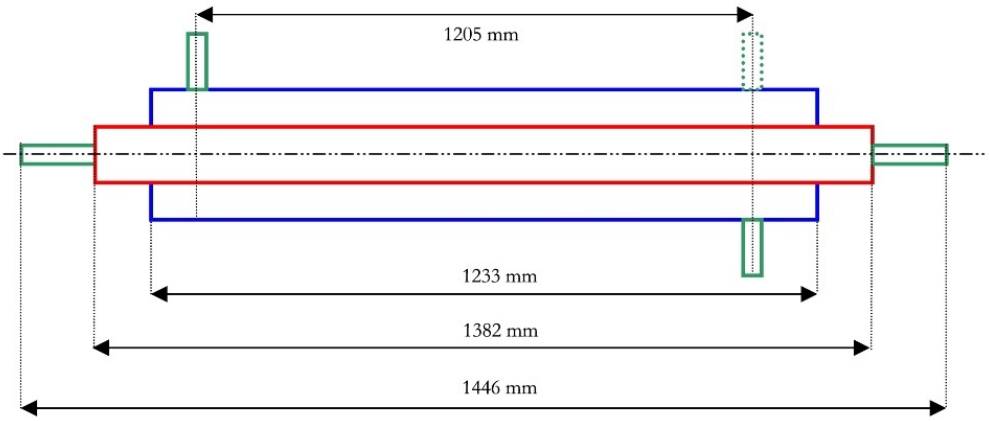

Figure 1. Scheme of coaxial HEX.

The heat transfer areas are:
Internal area–internal tube: 0.07747 m^2
External area–internal tube: 0.08522 m^2
Internal area–external tube: 0.1549 m^2
External area–external tube: 0.1627 m^2.

2.2. Experimental Setup

Figure 2 presents a scheme of the experimental setup.

The fluids are compressed air delivered at a relative pressure of 8 bars. Part of this air is delivered in the external part of the HEX. The other part passes through the DRAGON apparatus, from FROILABO [47]. This dry air could be delivered at the entrance of the HEX with a temperature in the range $[-80\ °C\ ;\ +250\ °C]$, the volumetric rate range is $[8\ Nm^3h^{-1}\ ;\ 30\ Nm^3h^{-1}]$. DRAGON apparatus allows fast temperature change in the range $[0.03\ °Cs^{-1}\ ;\ 20\ °Cs^{-1}]$. For example, the increase of the internal tube inlet temperature from $-55\ °C$ to $+125\ °C$ takes 7 s.

Air properties are available by means of the ELX (CNES software) except for conductivity and viscosity for which the data from Air Liquide encyclopedia are preferred [48].

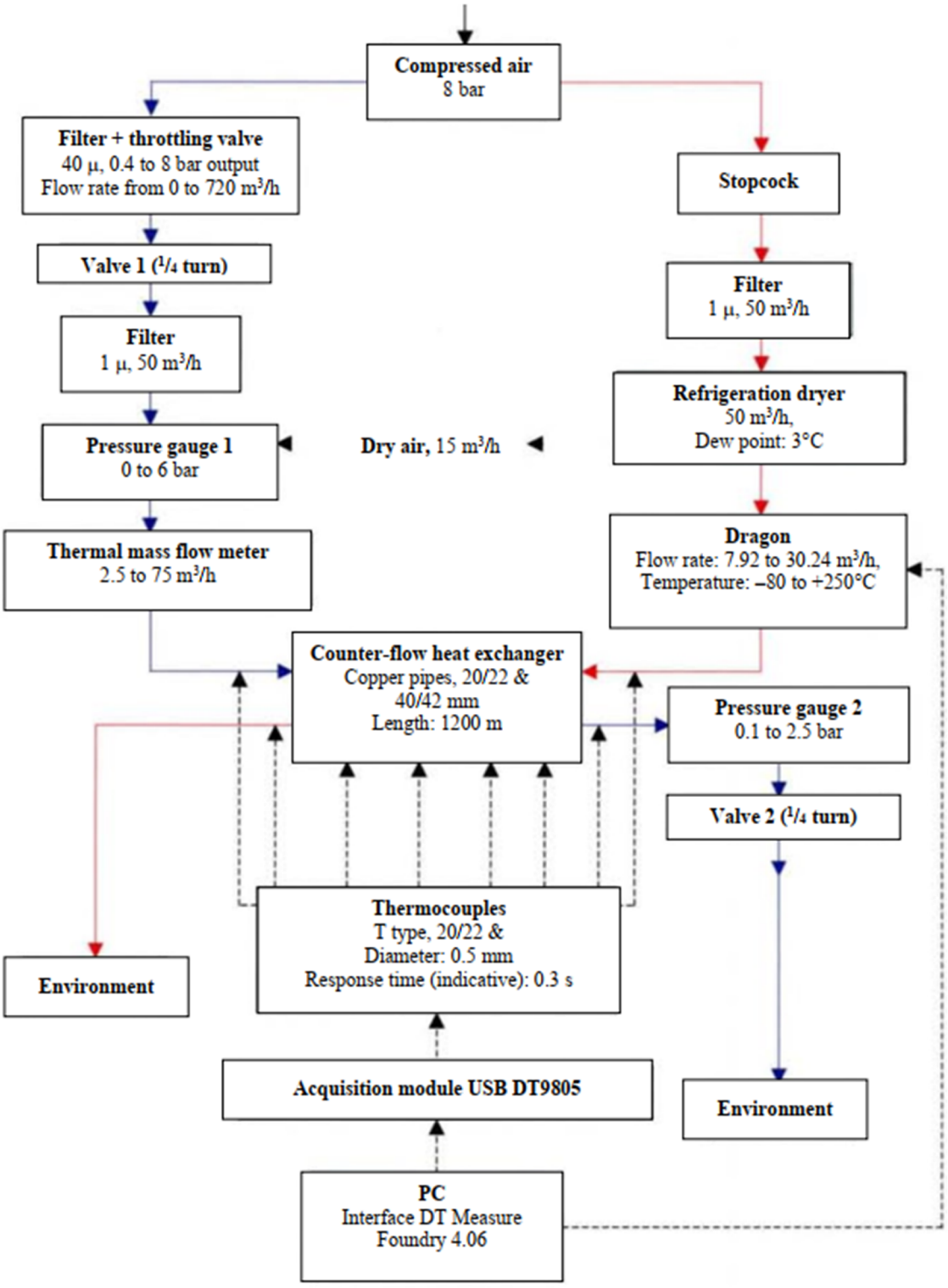

Figure 2. Scheme of the experimental setup.

2.2.1. Measurements

The lumped experimental analysis needs only four temperature measurements for which thermocouples are employed, with an accuracy of ± 0.5 °C in the range $[-40\ °C\ ;\ +125\ °C]$, and relaxation time of 0.03 s in liquids [49].

The mass flow rates are measured by two flow meters. Thus, the internal fluid flow rate is measured by a flow meter incorporated in the DRAGON, while the external fluid flow rate is measured by a mass flow meter INSTRUTEC—BRONKHORST HI TEC [50]. The similarity between the two measurements allows obtaining the characteristics of the second device: accuracy $\pm 0.5\%$ of the data $\pm 0.1\%$ of full scale in the range $[2.5\ \mathrm{Nm^3h^{-1}};\ 7.5\ \mathrm{Nm^3h^{-1}}]$; the time constant of the device is in the range $[1_s\,;\ 2_s]$.

2.2.2. Data Acquisition and Treatment

Data acquisition is performed using a DT 9805 card from SAIS—DATATRANSLATION [51]. Data processing is supervised by DT Measure Foundry program, also from DATATRANSLATION, using a PC.

The accuracy of $\dot{q}_i$ results is obtained according to Moffat [52]. For example, for the heat flux P transferred from fluid i, we use:

$$P_i = \dot{m}_i C_p \, (T_{ie} - T_{is}) \tag{2}$$

We neglect the uncertainty corresponding to C_p, issued from existing data for dry air, thus the relative uncertainty of P_i becomes:

$$\frac{dP_i}{P_i} = \sqrt{\left(\frac{d\dot{m}_i}{\dot{m}_i}\right)^2 + \left(\frac{dT_{ie} + dT_{is}}{T_{ie} - T_{is}}\right)^2} \tag{3}$$

Uncertainties will be emphasized on figures in Section 3.

2.3. Reported Experiments

A complete calibration of the experimental bench has been performed [42], during which some limitations of the planned experiences appeared: the present configuration of the setup does not allow step with negative temperature variation due to moisture presence in internal fluid. Dragon regulation and control do not allow imposing a step variation of the internal fluid mass flow rate, because the variation of mass flow rate and temperature are correlated. (but the internal mass flux could be an experiment parameter).

To study the turbulent-turbulent flow configuration, the internal fluid must be the primary one coming from DRAGON, and the external fluid, the secondary one (compressed air). The corresponding inlet temperature of the external fluid remains the ambient temperature. The most important influence of temperature T and pressure Pr conditions occurs on air density (Figure 3).

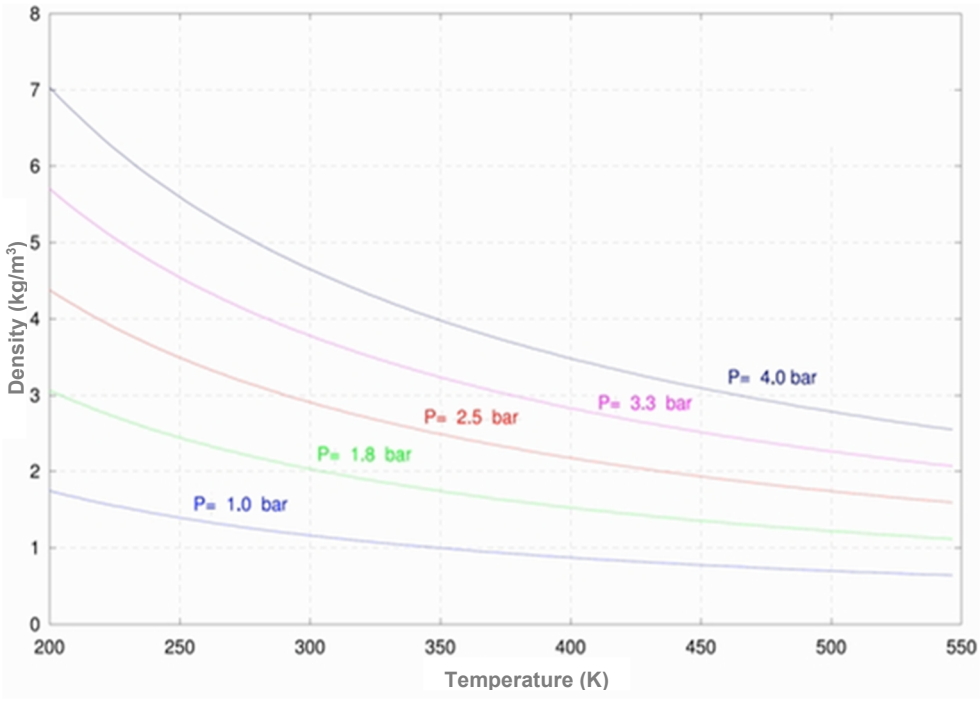

Figure 3. Air density variation with temperature and pressure.

Therefore, experiments are performed with minimal pressure losses. (ΔPr = 1.9 bar at maximum volumetric external flow rate of 62 Nm^3h^{-1}). Anyway, the density $\rho(Pr, T)$ is accurately calculated by means of the ELX software.

We will present hereafter the results that were obtained corresponding to the following experimental plan:

- ❖ parallel- and counter-flow configuration of HEX
- ❖ internal fluid volumetric flow rate, from 3 to 8 NLs^{-1}
- ❖ internal fluid inlet temperature, from −50 °C to +140 °C
- ❖ external fluid volumetric flow rate, from 29 to 62 Nm^3h^{-1}
- ❖ external fluid inlet temperature, from 20–25 °C (ambiance fluctuation)

The transient conditions are of step kind:

- ❖ increasing or Decreasing internal fluid temperature
- ❖ increasing or decreasing external fluid mass flow rate (through vane positioning).

3. Lumped System Analysis: Basic Results for HEX

This section considers successively a positive (respectively negative) temperature variation for the internal fluid, and a positive (respectively negative) mass flow rate variation for the external fluid.

3.1. Increasing Temperature Step for the Internal Fluid

The imposed temperature transient condition is a step increase of the internal fluid inlet temperature T_{inte}, from 60 °C to 120 °C, all other parameters being kept constant, as follows:

$$\dot{V}_{int} = 18\ Nm^3h^{-1};\ \dot{V}_{ext} = 35\ Nm^3h^{-1};\ Pr_{exte} = 3\ bar;\ Pr_{exts} = 1.46\ bar;\ T_{exte} = 26.3\ °C.$$

The ambient temperature is 23.5 °C, so the quasi-adiabatic condition is fulfilled. Figures 4 and 5 illustrate the evolution in time of the exit temperatures of the internal and external fluid.

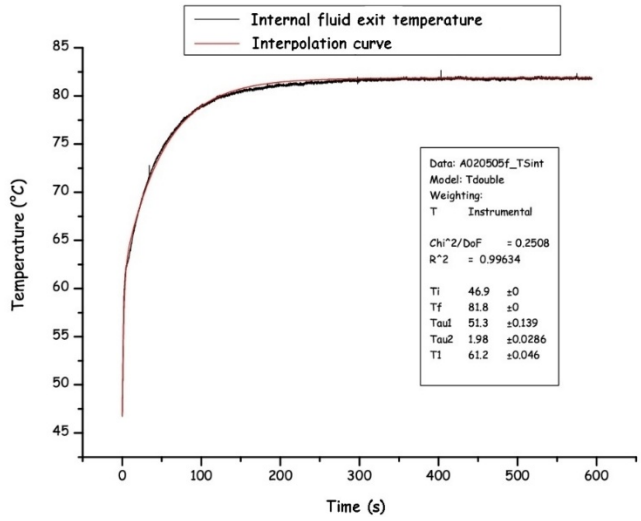

Figure 4. Internal fluid exit temperature variation in time.

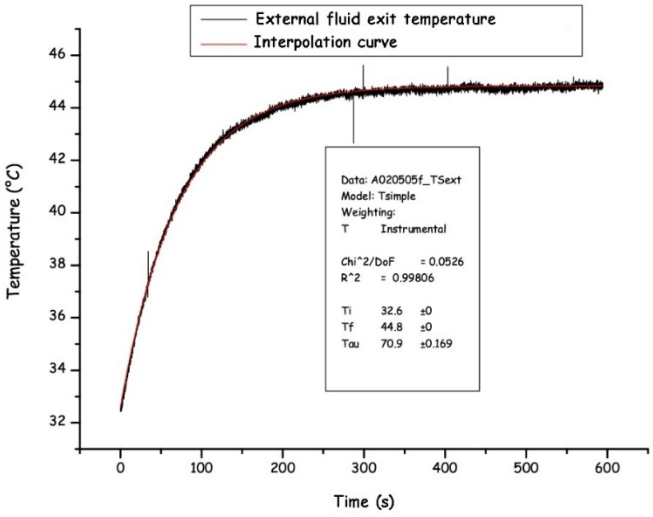

Figure 5. External fluid exit temperature variation in time.

For the internal fluid, a specific moment occurs that corresponds to a discontinuity in the slope of the T_{ints} curve.

Figure 6 shows a magnified view of this discontinuity due to imperfect temperature step. This can be explained by the presence of an overlap and the finite temperature increase (25 °Cs^{-1}) (Figure 7).

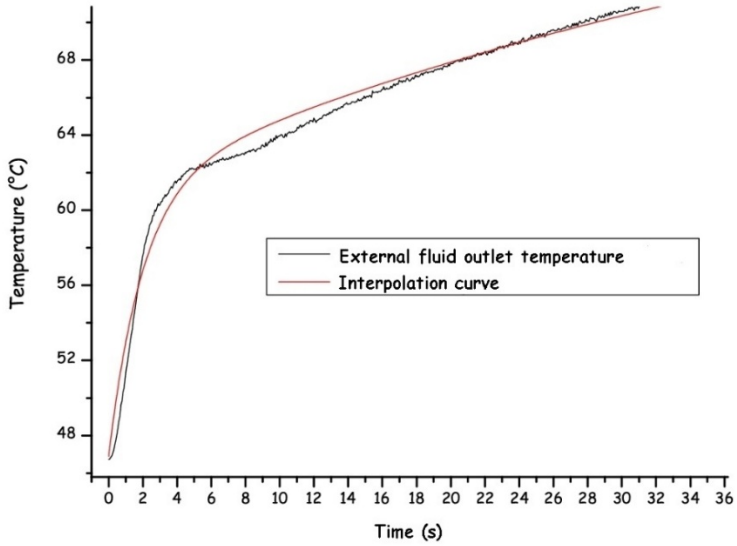

Figure 6. External fluid temperature at the outlet in the first seconds.

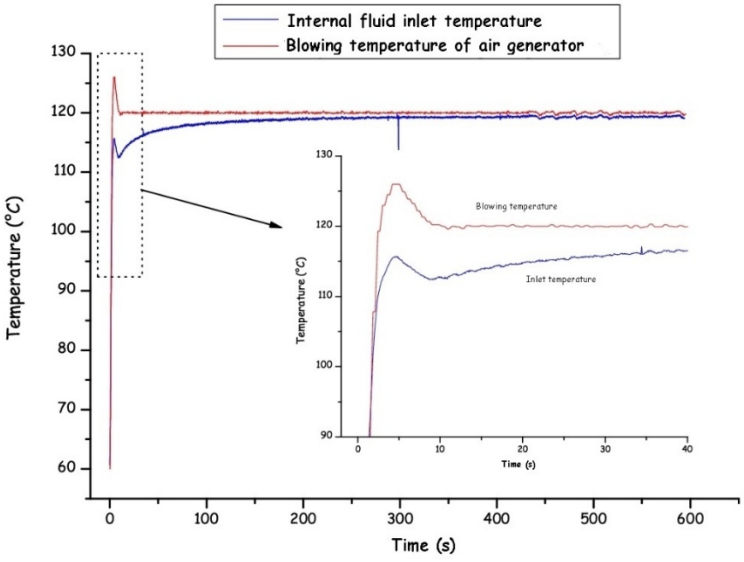

Figure 7. Internal fluid inlet temperature as a function of time.

3.1.1. Perturbed Temperature Response at Fluid Exit

In conclusion, with these observations, it appears that the temperature responses of the system are representative of the HEX, but also for the perturbed fluid. Thus, a time constant at short time is related to imperfect perturbation, while a time constant at long time characterizes the thermal response of the studied system. Consequently, the model must include for the exit temperature of the perturbed fluid a bi-exponential function due to the low thermal inertia of the gas, compared to the liquid commonly studied so far:

$$\begin{cases} T_{\text{ints}}(t) = T_{\text{ints}}^{o}, \text{ if } t \le t_o \\ T_{\text{ints}}(t) = T_{\text{ints}}^{\infty} + (T_1 - T_{\text{ints}}^{\infty})\exp\left(-\dfrac{t}{\tau_{\text{int}L}}\right) + (T_{\text{ints}}^{0} - T_1)\exp\left(-\dfrac{t}{\tau_{\text{int}C}}\right), \text{ if } t > t_o \end{cases} \quad (4)$$

The curve fitting was obtained with ORIGIN program. According to Equation (4), the best solution associated with Figure 4 corresponds to:

$$T_{\text{ints}}^{o} = 46.9\ °\text{C}\ ;\ T_{\text{ints}}^{\infty} = 81.8\ °\text{C}\ ;\ T_1 = 81.8\ °\text{C}$$

$$\tau_{\text{int L}} = 51.3 \pm 0.1\text{s} \ ; \ \tau_{\text{int C}} = 1.98 \pm 0.03\text{s}$$

where T_1 represents a transition temperature.

This transition temperature seems more appropriate here than a time lag. We note that $T^o_{\text{int}s}$ and $T^\infty_{\text{int}s}$ are parameters, as in the case of liquid-liquid HEX.

3.1.2. Non-Perturbed Fluid Exit Temperature Response

For the non-perturbed external fluid, an exponential curve fitting is sufficient and representative for the experiments, as the imperfect perturbation is smoothed by the HEX system (material inertia). According to Equation (1), we obtain:

$$T^o_{\text{ext}s} = 32.6\ ^\circ\text{C} \ ; \ T^\infty_{\text{ext}s} = 44.8\ ^\circ\text{C} \ ; \ \tau_{\text{ext}} = 70.9 \pm 0.2\ \text{s}$$

The important and corresponding new result is that the time constants are different for the internal (perturbed) and external fluid (51.3 s ≠ 70.9 s). This clearly shows that gas-gas HEX behavior differs from that of liquid-liquid HEX that requires a single time constant for the two fluids, as mentioned in the literature.

This can be explained by the low inertia of the gaseous fluids compared to the inertia of the tube material. For liquid-liquid HEX, the inertia of the fluids is the same order of magnitude as that of the tubes. The standard model (relative to liquids) gives a time constant τ = 30.2 s, smaller than the observed values. Consequently, it seems that the models proposed for liquid-liquid HEX are inadequate for gas-gas HEX.

3.1.3. Transient Heat Fluxes Transmitted (Extensive Quantities)

These heat transfer rates or fluxes *P* are calculated according to Equation (2). Figure 8 shows that the HEX thermal response corresponds to long time constants.

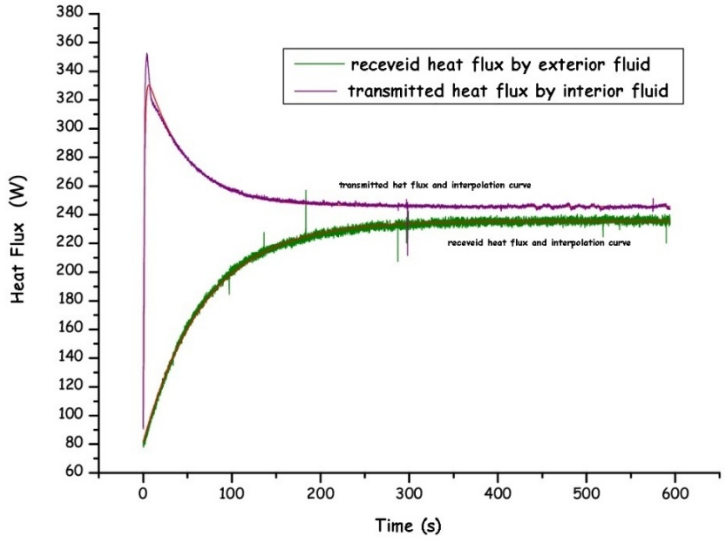

Figure 8. Transient heat fluxes P as a function of time.

Logically, the heat flux *P* transmitted by the internal (perturbed) fluid is fitted by two exponential forms, while the external fluid received heat flux is represented by an exponential formula. We use:

$$P^o_{\text{int}} = 90.7\ \text{W} \ ; \ P^\infty_{\text{int}} = 246\ \text{W} \ ; \ P_1 = 346 \pm 1\ \text{W}$$

$$P^o_{\text{int}} = 90.7\ \text{W} \ ; \ P^\infty_{\text{int}} = 246\ \text{W} \ ; \ P_1 = 346 \pm 1\ \text{W}$$

$$P^o_{\text{ext}} = 81.7\ \text{W} \ ; \ P^\infty_{\text{ext}} = 236\ \text{W} \ ; \ \tau_{\text{Pext}} = 69.8 \pm 0.4\ \text{s}$$

It is observed that the thermal insulation corresponds to a heat loss of 4% in the final state, and 11% in the initial state. Then, $\tau_{\text{int}L}$ differs from $\tau_{\text{Pint}L}$ by about 10%, while τ_{ext} is very close to τ_{Pext}, as expected.

The transient power differential, *DP*, is representative of the tubes inertia. Figure 9 confirms the need of a two exponentials fit. In this case, we have:

$$DP^0 = 9.0\ \text{W}\ ;\ DP^\infty = 9.9\ \text{W}\ ;\ \text{DP}_1 = 262 \pm 2\ \text{W}$$

$$\tau_{\text{DP}L} = 60.2 \pm 0.5\ \text{s}\ ;\ \tau_{\text{DP}C} = 60.2 \pm 0.05\ \text{s}$$

We note that $\tau_{\text{DP}L}$ is in between the different time constants relative to the internal and external fluids.

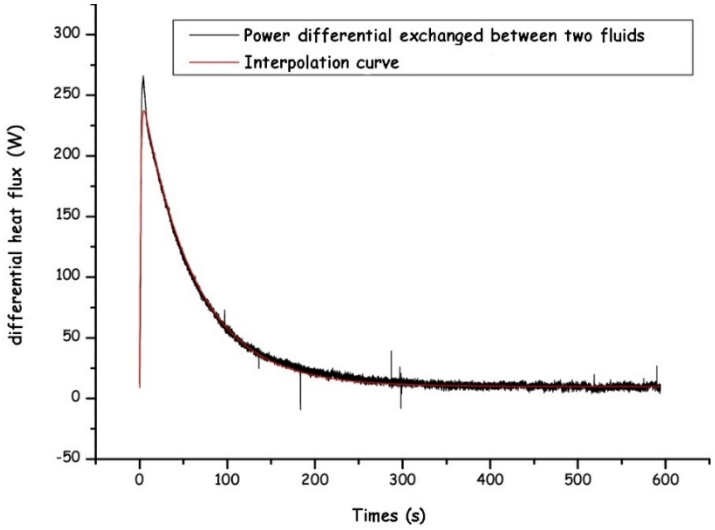

Figure 9. Transient differential heat flux *DP* versus as a function of time.

3.2. Decrease in Internal Fluid Temperature by Step-Type Variation

During the decreasing temperature perturbation of T_{ie}, the internal fluid inlet temperature starts from 140 °C to go down to 80 °C. All other parameters remain constant at the same values indicated in Section 3.1, except for T_{exte} = 26.6 °C. Thus, the absolute value of the step ΔT is preserved.

The same method as previously (Section 3.1) is applied [42], and the following results are obtained for the exit temperatures:

❖ Internal perturbed fluid

$$T^o_{\text{ints}} = 93.4\ ^\circ\text{C}\ ;\ T^\infty_{\text{ints}} = 58.7\ ^\circ\text{C}\ ;\ T_1 = (79.1 \pm 0.1)\ ^\circ\text{C}$$

$$\tau_{\text{int}L} = 51.4 \pm 0.2\ \text{s}\ ;\ \tau_{\text{int}C} = 4.52 \pm 0.05\ \text{s}$$

❖ External fluid

$$T^o_{\text{exts}} = 49.0\ ^\circ\text{C}\ ;\ T^\infty_{\text{exts}} = 38.9\ ^\circ\text{C}\ ;\ \tau_{\text{ext}} = 70.8 \pm 0.2\ \text{s}$$

We observe from these results that, for a given absolute value of ΔT, the sign of the variation has no significant influence on the time constant at long time.

Then, the method is applied to the corresponding transient heat fluxes *P* and we obtain under the same conditions for temperatures:

$$P^o_{\text{int}} = 297\ \text{W}\ ;\ P^\infty_{\text{int}} = 141\ \text{W}\ ;\ P_1 = 26.3 \pm 0.8\ \text{W}$$

$$\tau_{\text{P}\text{int}L} = 45.3 \pm 0.4\ \text{s}\ ;\ \tau_{\text{P}\text{int}C} = 2.65 \pm 0.03\ \text{s}$$

$$P^o_{\text{ext}} = 284\ \text{W}\ ;\ P^\infty_{\text{ext}} = 131\ \text{W}\ ;\ \tau_{\text{Pext}} = 72.1 \pm 0.4\ \text{s}$$

$$\text{DP}^o = 13.3\ \text{W}\ ;\ \text{DP}^\infty = 10.3\ \text{W}\ ;\ \text{DP}_1 = -249 \pm 24\ \text{W}$$

$$\tau_{\text{DP}L} = 60.1 \pm 0.5\ \text{s}\ ;\ \tau_{\text{DP}C} = 2.65 \pm 0.08\ \text{s}$$

Thus, the conclusions are identical in terms of heat fluxes and temperatures, only T_1, P_1 and τ_C are different.

3.3. Positive Variation of the External Fluid Mass Flux

This variation, that is mechanically rapid compared to the thermal response, simultaneously influences the variation (step) of the mass flow rate, as well as the changes of the inlet and exit pressure of external flow. The conditions of the experiment described in this section are as follows:

$$T_{inte} = 120\ °C\ ;\ T_{exte} = 25\ °C\ ;\ T_{amb} = 22.3\ °C$$

$$\dot{V}_{int} = 18\ Nm^3h^{-1}\ ;\ \dot{V}_{ext}^{0} = 29.9\ Nm^3h^{-1}\ ;\ \dot{V}_{ext}^{\infty} = 58.8\ Nm^3h^{-1}$$

With the step-type mass flow rate variation, the external fluid inlet pressure (respectively exit pressure) varies from

$$Pr_{exte}^{o} = 2.65\ \text{bar to}\ Pr_{exte}^{\infty} = 4.8\ \text{bar, respectively from}$$

$$Pr_{exts}^{o} = 1.35\ \text{bar to}\ Pr_{exts}^{\infty} = 2\ \text{bar.}$$

The treatment of the experimental data shows this time that a single exponential fit is sufficient for the internal (non-perturbed) fluid but, at the same time a two exponential fitting is necessary for the perturbed external fluid. This seems to be primarily related to the perturbed fluid itself, but also to the important variation of the perturbed fluid inlet temperature, with a short response time (coupled heat and mass transfer phenomena for the counter-flow configuration). During the experiment, we noticed a glide of the external fluid inlet temperature of almost 1 °C.

3.3.1. Temperature Response

The results obtained are as follows:

$$T_{exts}^{o} = 45.5\ °C\ ;\ T_{exts}^{\infty} = 37.7\ °C\ ;\ T_1 = 43.5 \pm 0.1\ s$$

$$\tau_{extL} = 35.3 \pm 0.5\ s\ ;\ \tau_{extC} = 2.11 \pm 0.23\ s$$

$$T_{ints}^{o} = 83.2\ °C\ ;\ T_{ints}^{\infty} = 75.4\ °C\ ;\ \tau_{int} = 33.1 \pm 0.2\ s$$

We observe that the difference between the two time constants of the fluids is less important in this case (7% in Section 3.3) than for temperature perturbation. The time constant given by the standard model (τ = 31.24 s) is also relatively close to the two experimental ones, especially for the non-perturbed fluid.

3.3.2. Heat Flux Response

The transient response for heat fluxes is fitted for the same conditions as in Section 3.3.1. The results obtained are:

$$P_{int}^{o} = 237\ W\ ;\ P_{int}^{\infty} = 285\ W\ ;\ \tau_{Pint} = 31.2 \pm 0.6\ s$$

$$P_{ext}^{o} = 266\ W\ ;\ P_{ext}^{\infty} = 457\ W\ ;\ P_1 = 396 \pm 2\ W$$

$$\tau_{PextL} = 45.8 \pm 1\ s\ ;\ \tau_{PextC} = 1.45 \pm 0.24\ s$$

$$DP^{o} = -220\ W\ ;\ DP^{\infty} = 13.3\ W\ ;\ DP_1 = -159 \pm 3\ W$$

$$\tau_{DPL} = 41.4\ s\ ;\ \tau_{DPC} = 1.52 \pm 0.36\ s$$

We notice here a 25% difference between the temperature time constant and power time constant of the external (perturbed) fluid: $\tau_{PextL} > \tau_{extL}$.

3.4. Negative Variation of External Mass Flow Rate

The decrease in mass flow rate remains associated with the variation of the inlet and exit pressures of the external fluid. The experimental conditions are as follows:

$$T_{inte} = 120\ °C\ ;\ T_{exte} = 25.1\ °C\ ;\ T_{amb} = 22.5\ °C$$

$$\dot{V}_{int} = 18\ Nm^3h^{-1};\ \dot{V}_{ext}^{0} = 58.7\ Nm^3h^{-1};\ \dot{V}_{ext}^{\infty} = 29.3\ Nm^3h^{-1}$$

$$(Pr_{exte}^{o} = 4.8\ \text{bar}\ ;\ Pr_{exte}^{\infty} = 2.6\ \text{bar}\ ;\ Pr_{exts}^{o} = 2\ \text{bar}\ ;\ Pr_{exts}^{\infty} = 1.35\ \text{bar})$$

3.4.1. Temperature Response

The temperature data fitting gives:

$$T^{o}_{\text{exts}} = 37\ ^{\circ}\text{C}\ ;\ T^{\infty}_{\text{exte}} = 46.2\ ^{\circ}\text{C}\ ;\ T_1 = 39.9 \pm 0.1\ ^{\circ}\text{C}$$

$$\tau_{\text{ext}L} = 61.9 \pm 0.7\ \text{s}\ ;\ \tau_{\text{ext}C} = 4.43 \pm 0.4\ \text{s}$$

$$T^{o}_{\text{ints}} = 75.5\ ^{\circ}\text{C}\ ;\ T^{\infty}_{\text{ints}} = 83.6\ ^{\circ}\text{C}\ ;\ \tau_{\text{int}} = 44.9 \pm 0.2\ \text{s}$$

Here we notice a very large difference between the two temperature time constants (essential difference from the results of Section 3.3.1). These two time constants are also higher. The time constant provided by the standard model (48.3 s) is slightly bigger than the time constant obtained experimentally for the non-perturbed fluid.

3.4.2. Heat Flux Response

Under the same conditions as those indicated in Section 3.4.1, the fitting gives the following results:

$$P^{o}_{\text{int}} = 285\ \text{W}\ ;\ P^{\infty}_{\text{int}} = 233\ \text{W}\ ;\ \tau_{\text{Pint}} = 43.5 \pm 0.6\ \text{s}$$

$$P^{o}_{\text{ext}} = 134\ \text{W}\ ;\ P^{\infty}_{\text{ext}} = 230\ \text{W}\ ;\ P_1 = 148 \pm 1\ \text{W}$$

$$\tau_{\text{Pext}L} = 75.9 \pm 1.4\ \text{s}\ ;\ \tau_{\text{Pext}C} = 4.18 \pm 0.58\ \text{s}$$

$$DP^{o} = 152\ \text{W}\ ;\ DP^{\infty} = -3.86\ \text{W}\ ;\ DP_1 = 121 \pm 3\ \text{W}$$

$$\tau_{\text{DP}L} = 63.6 \pm 1.6\ \text{s}\ ;\ \tau_{\text{DP}C} = 5.96 \pm 1.18\ \text{s}$$

We again observe a significant difference between the two heat power time constants, with the heat flux time constant conserving 25% more than the temperature time constant for the perturbed fluid. The differential heat flux time constant has an intermediate value between $\tau_{\text{Pext}L}$ and τ_{Pint}.

4. Sensivity Analysis of the HEX Time Constants with Respect to Internal Temperature Perturbation

This section presents to the results of an experimental study on the influence of main experimental parameters on the time constants, for transient ΔT_i and HEX parameters (parallel-and counter-flow configurations; $\dot{V}_{\text{int}}$; $\dot{V}_{\text{ext}}$; T_{inte}), with the exception of the HEX geometry. Only the long time constant is considered for the perturbed fluid.

4.1. Sensitivity of Time Constants to ΔT_i

The step-type temperature variation is applied to the internal fluid according to the procedure described in Section 2. The tested ΔT variation is positive or negative and is relative to the two HEX configurations.

The experimental results show no significant difference in τ for $|\Delta T|$ >10 °C. The same conclusion applies to τ_P, but with slightly more dispersed results due to the propagation of uncertainties. It is observed that τ_{Pext} for the decrease in temperature is greater than τ_{Pext} for the increase in temperature. Time constant for the perturbed fluid is lower (30%) than that for the non-perturbed fluid, while τ_{DP} exhibits intermediate values. The time constant calculated by the proposed method for liquids gives an estimation significantly lower than the observed values (but also independent of ΔT).

4.2. Sensitivity of Time Constants to $\dot{V}_{int}$

Figure 10 confirms the strong influence of $\dot{V}_{\text{int}}$, the internal fluid flow rate, which diminishes every time constant. It appears that experiments with decreasing temperature step exhibit a slightly faster decrease of the temperature time constant than at temperature step increase, with a crossing point of the two curves. The heat flux time constant is higher temperature step decrease than during the temperature step increase [42]. No significant difference is noted relative to τ_{DP}, the differential heat flux constant.

Finally, we observe that the time constants for parallel-flow are greater than those for counter-flow HEX.

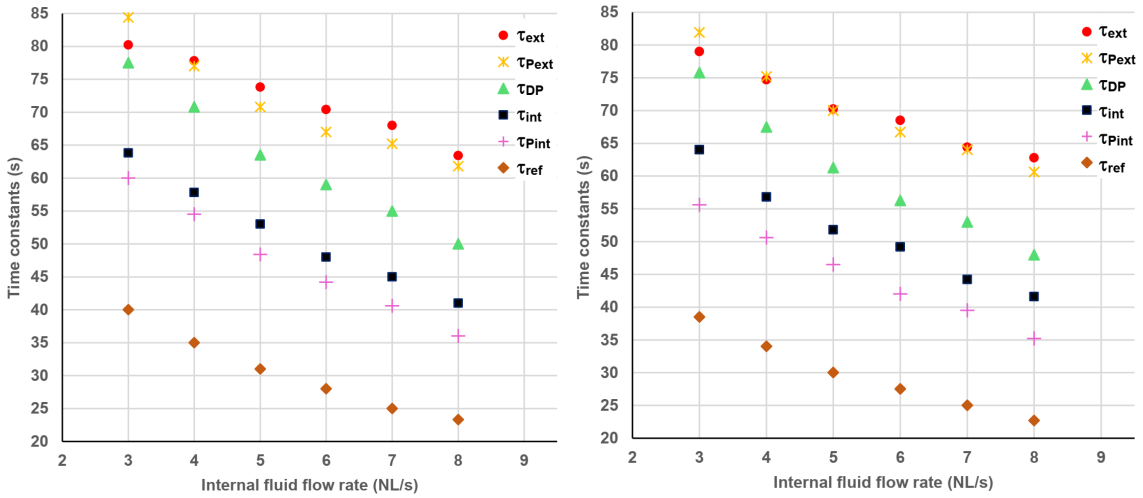

Figure 10. Time constants variation with internal flow rate, for parallel-flow (**left**) and counter-flow (**right**) HEX (temperature perturbation).

4.3. Sensitivity of Time Constants to $\dot{V}_{ext}$

The external fluid flow rate also exerts a strong influence on each time constant, but particularly on the time constants of the external (perturbed) fluid, see Figure 11. The influence of fluid flow rates on the convective heat transfer coefficients can explain the two strong influences on the time constants observed in Sections 4.2 and 4.3. The weak influence of the sign of the temperature disturbance is confirmed, as is that of the HEX configuration, with the exception of the time constant of the internal fluid heat flux ($\tau_{P\text{counter-flow}} < \tau_{P\text{parallel-flow}}$).

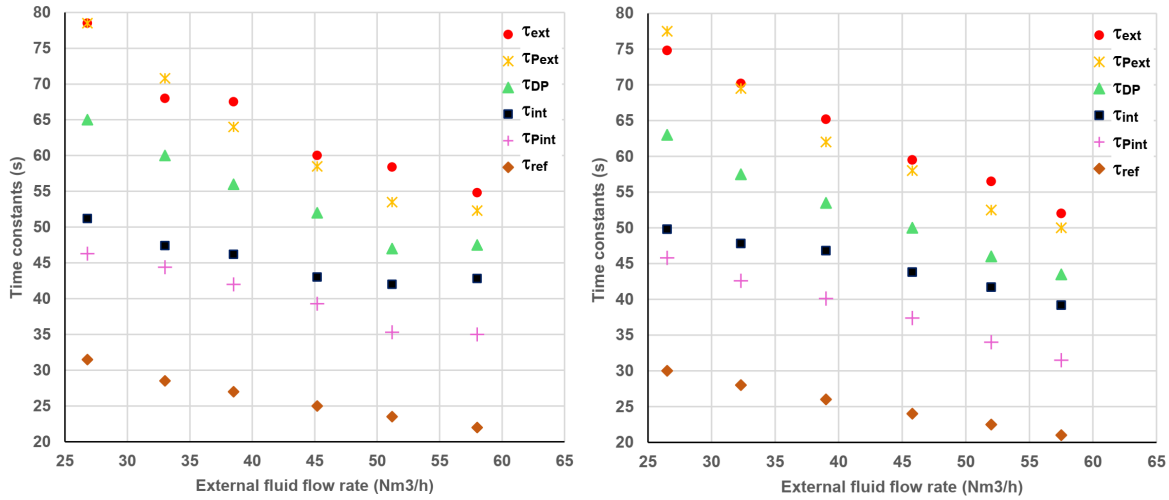

Figure 11. Time constants as a function of external fluid flow rate, for parallel-flow (**left**) and counter-flow (**right**) HEX relative to temperature perturbation.

To conclude the sensitivity analysis of the temperature perturbation, the main observations are the strong influence of the mass flow rates of the internal and external fluids, compared to the weak influence of the sign of the temperature perturbation, as well as the HEX configuration.

5. Sensivity Analysis of the HEX Time Constants with Respect to External Fluid Flow Rate Perturbation

This study is similar to previous one, but replaces ΔT_{int}, the internal fluid temperature perturbation, with $\Delta\dot{V}_{\text{ext}}$, the external fluid flow rate perturbation. Only the long time constant is considered for the perturbed fluid.

5.1. Sensitivity of Time Constants to $\Delta\dot{V}_{ext}$

The mass flow rate step is carried out on the external fluid in accordance with the procedure in Section 2. The tested variations $\Delta\dot{V}_{\text{ext}}$ are positive ones ($\dot{V}_{\text{ext}}^{0}$ = 29.4 Nm^3h^{-1}; $\dot{V}_{\text{ext}}^{\infty}$ = 41.6 to 57.5 Nm^3h^{-1}) or negative ($\dot{V}_{\text{ext}}^{0}$= 57.9 Nm^3h^{-1}; $\dot{V}_{\text{ext}}^{\infty}$= 49.4 to 29.7 Nm^3h^{-1}).

Experimental results indicate that the sign of the perturbation strongly influence the system response. Thus, an increase in $\Delta\dot{V}_{\text{ext}}$ decreases every time constant, while a decrease in $\Delta\dot{V}_{\text{ext}}$ increases them.

The intersection points of the corresponding curves are located at 16 Nm^3h^{-1} for the heat power time constants and around 12.5 Nm^3h^{-1} for the temperature time constants.

The time constants of the external fluid are higher than those of the internal fluid in terms of transmitted heat rate (τ_{DP} is intermediate). The time constants of the reference model remain the lowest, but the general trend is maintained.

Comparison of Parallel- and Counter-Flow Configurations

Figure 12 corresponds to the following experimental conditions and to the increase in $\Delta\dot{V}_{\text{ext}}$:

$$T_{\text{inte}} = 120\ °\text{C}\ ;\ T_{\text{amb}} = 22.4 - 23.3\ °\text{C}$$

$$T_{\text{exte}} = \begin{cases} 24.5 - 25.5\ °\text{C} & \text{for counter-flow} \\ 23 - 24.6\ °\text{C} & \text{for parallel-flow} \end{cases}$$

$$\dot{V}_{\text{int}} = 21.6\ \text{Nm}^3 \cdot \text{h}^{-1}\ ;\ \dot{V}_{\text{ext}}^{0} = 29.4\ \text{Nm}^3 \cdot \text{h}^{-1}\ ;\ \dot{V}_{\text{ext}}^{\infty} = 41.4\ \text{to}\ 58.4\ \text{Nm}^3 \cdot \text{h}^{-1}$$

$$Pr_{\text{exte}} = 26\ \text{to}\ 4.8\ \text{bar}\ ;\ Pr_{\text{exts}} = 1.35\ \text{to}\ 2\ \text{bar}$$

This figure shows a significant decrease of every time constant with $\Delta\dot{V}_{\text{ext}}$. Furthermore, the time constants in parallel-flow are greater than those in counter-flow. The influence is more pronounced on the heat transfer time constants than on the temperature time constants.

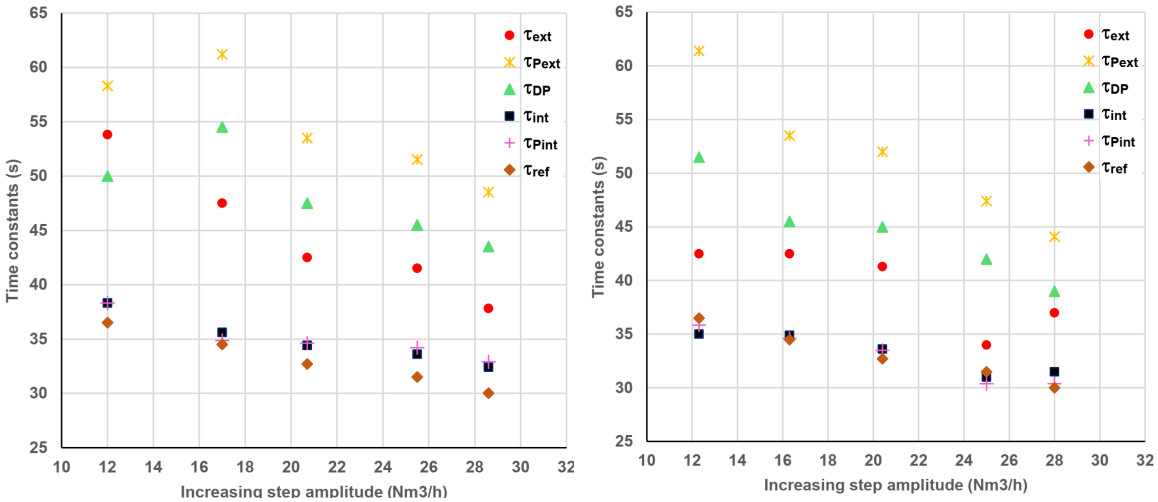

Figure 12. Time constants as a function of external fluid flow rate perturbation (increasing), for parallel-flow (**left**) and counter-flow (**right**) HEX.

For the experimental conditions mentioned above, Figure 13 illustrates the uncertainties associated with each time constant, as described in Section 2.2. The four graphs that comprise clearly show the decrease in all time constants as the perturbation of the external fluid flow increases. Furthermore, the uncertainty of the heat flux time constants, τ_{Pint} and τ_{Pext}, is significantly greater than that of the temperature constants, τ_{int} and τ_{ext}.

Figure 14 corresponds to the following similar experimental conditions and a decrease in $\dot{V}_{\text{ext}}$:

$$T_{\text{inte}} = 120\ °\text{C}\ ;\ T_{\text{amb}} = 22.9 - 23.4\ °\text{C}$$

$$\dot{V}_{\text{int}} = 21.6\ \text{Nm}^3\text{h}^{-1}\ ;\ \dot{V}_{\text{ext}}^{0} = 57.4\ \text{Nm}^3\text{h}^{-1}\ ;\ \dot{V}_{\text{ext}}^{\infty} = 49.6\ \text{to}\ 29.7\ \text{Nm}^3\text{h}^{-1}$$

$$\text{Pr}_{\text{exte}} = 2.6\ \text{to}\ 4.8\ \text{bar}\ ;\ \text{Pr}_{\text{exts}} = 1.35\ \text{to}\ 2\ \text{bar}$$

This time, we observe a significant increase in each time constant, and a small influence of HEX configuration (parallel- or counter-flow), except on the time constant of the internal fluid. We note that $\tau_{\text{int couter-flow}} > \tau_{\text{int parallel-flow}}$.

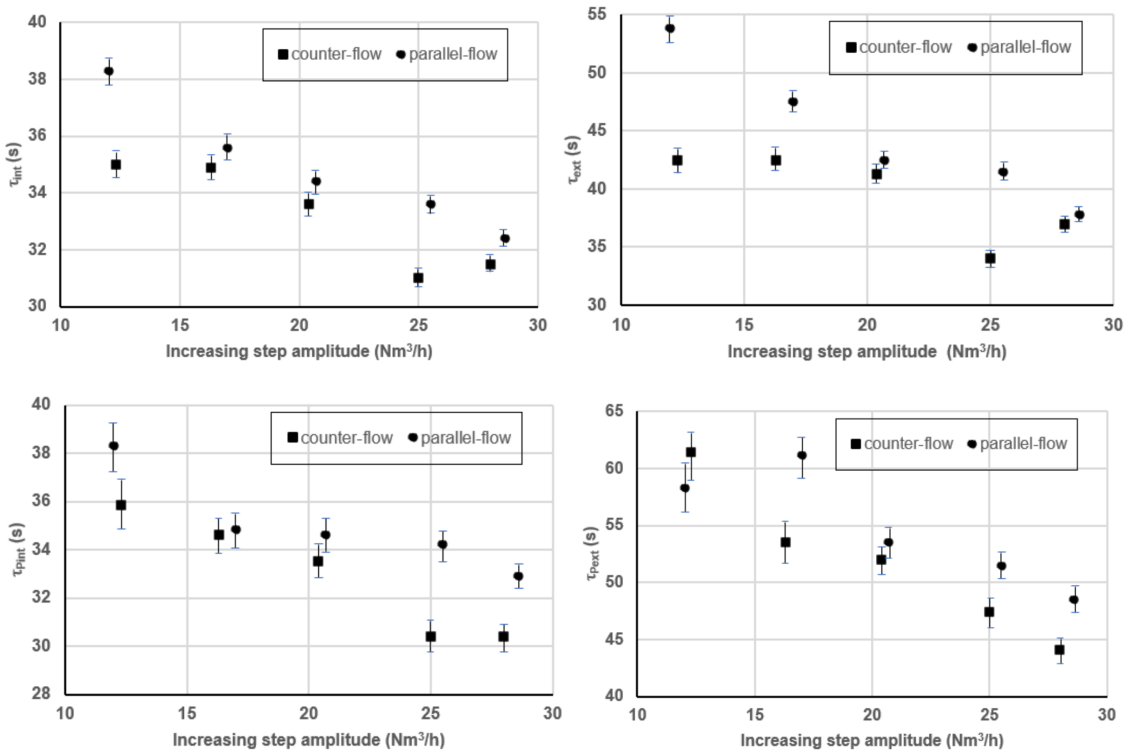

Figure 13. Time constants with uncertainties, as a function of external fluid flow rate perturbation (increasing).

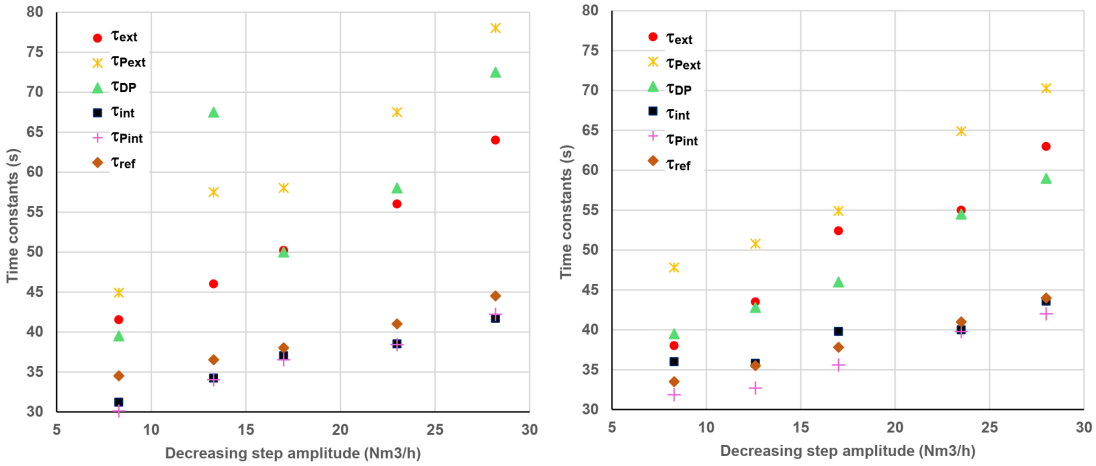

Figure 14. Time constants as a function of external fluid flow rate perturbation (decreasing), for parallel-flow (**left**) and counter-flow (**right**) HEX.

5.2. Influence of Internal Fluid Flow Rate $\dot{V}_{int}$

The reported experiments are performed by varying $\dot{V}_{\text{int}}$ at the maximum absolute volume for $\Delta\dot{V}_{\text{ext}}$. This results in a clear difference between increasing and decreasing perturbations of the external flow rate, regardless of the time constant considered. Furthermore, each time constant is a decreasing function of $\dot{V}_{\text{int}}$.

Comparison of Parallel- and Counter-Flow Configurations

Figures 15 and 16 present a comparison of the two HEX configurations for increasing (respectively decreasing) value of $\Delta\dot{V}_{\text{ext}}$, and the following experimental conditions:

$$T_{\text{inte}} = 120\ °\text{C}\ ;\ T_{\text{amb}} = 22.9 - 23.4\ °\text{C}$$

$$T_{\text{exte}} = \begin{cases} 24.5 - 26.9\ °\text{C for counter-flow} \\ 22.7 - 26.4\ °\text{C for parallel-flow} \end{cases}$$

$$\dot{V}_{\text{int}} = 10.8 - 28.8\ \text{Nm}^3\text{h}^{-1}\ ;\ \dot{V}_{\text{ext}}^{0} = 29.8 - 30.3\ \text{Nm}^3\text{h}^{-1}\ ;$$

$$\dot{V}_{\text{ext}}^{\infty} = 58.4 \text{ to } 58.7 \text{ Nm}^3\text{h}^{-1}$$

$$Pr_{exte} = 2.6 \text{ to } 4.8 \text{ bar} \; ; \; Pr_{exts} = 1.35 \text{ to } 2 \text{ bar}$$

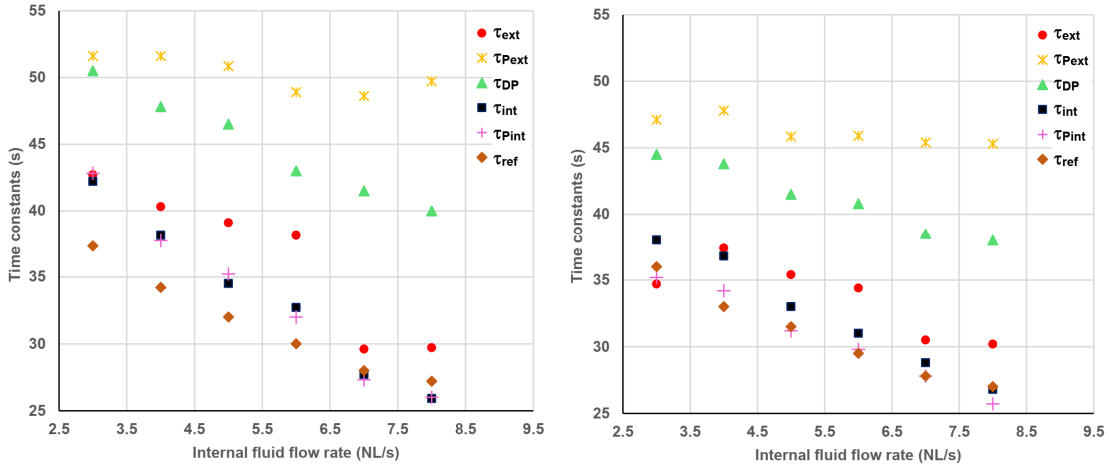

Figure 15. Time constants as a function of internal fluid flow rate, for a positive external fluid flow rate step, for parallel-flow (**left**) and counter-flow (**right**) HEX.

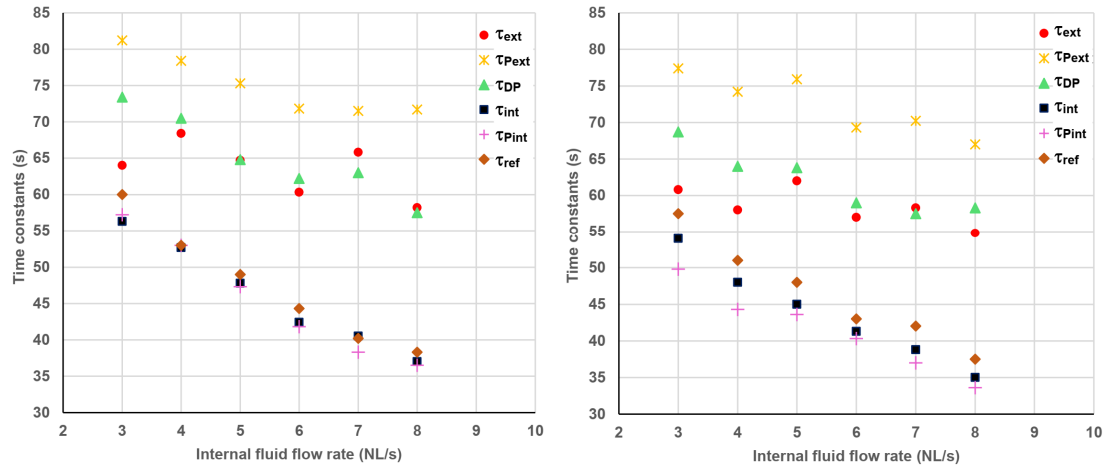

Figure 16. Time constants as a function of internal fluid flow rate, for a negative external fluid flow rate step, for parallel-flow (**left**) and counter-flow (**right**) HEX.

For each case, we observe decreasing values of the time constants τ, with $\tau_{\text{parallel-flow}} > \tau_{\text{couter-flow}}$.

5.3. Influence of the Internal Fluid Inlet Temperature T_{inte}

This influence is illustrated in Figure 17 for the counter-flow HEX configuration, with a maximum positive or negative variation in the external fluid flow rate. The experimental conditions are as follows:

$$T_{\text{inte}} = 60 \text{ to } 140 \text{ °C} \; ; \; T_{\text{amb}} = 22.9 - 23.1 \text{ °C}$$

$$T_{\text{exte}} = \begin{cases} 24.6 - 26.3 \text{ °C} & \text{for decreasing step} \\ 23.8 - 26.1 \text{ °C} & \text{for increasing step} \end{cases}$$

$$\dot{V}_{\text{int}} = 21.6 \text{Nm}^3 \cdot h^{-1}$$

$$\dot{V}_{\text{ext}}^{0} = \begin{cases} 29.3 - 30.1 \text{ Nm}^3\text{h}^{-1} & \text{increasing step} \\ 57.9 - 59.2 \text{ Nm}^3\text{h}^{-1} & \text{decreasing step} \end{cases}$$

$$\dot{V}_{\text{ext}}^{\infty} = \begin{cases} 57.9 - 59.1 \text{ Nm}^3\text{h}^{-1} & \text{increasing step} \\ 29.3 - 30.1 \text{ Nm}^3\text{h}^{-1} & \text{decreasing step} \end{cases}$$

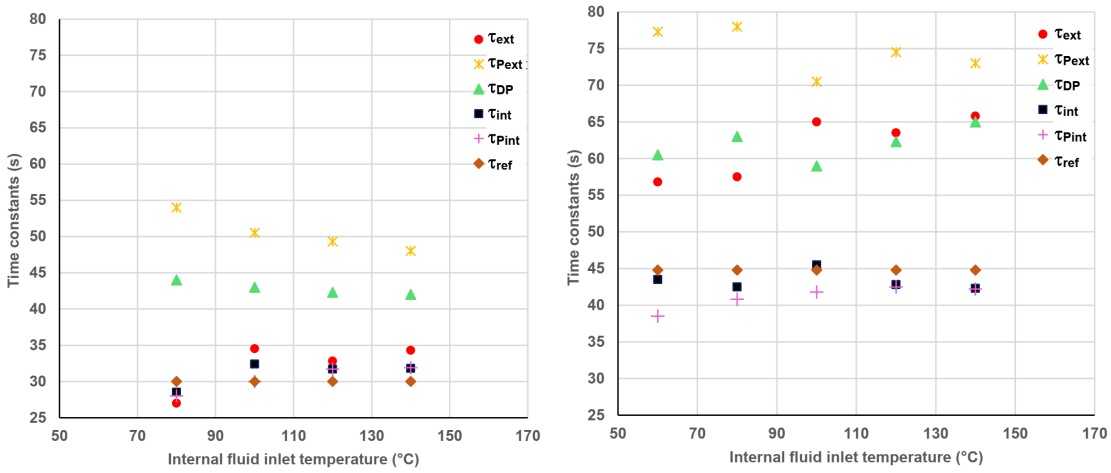

Figure 17. Time constant as a function of the inlet temperature of the internal fluid, for a positive (**left**) and negative (**right**) step variation of the external flow rate, for counter-flow HEX.

We observe that the influence of T_{inte} is indeed moderate. The difference between the decrease and increase in mass flow rate $\Delta\dot{V}_{ext}$ is more pronounced: $\tau_{decreasing} > \tau_{increasing}$. Furthermore, the difference between the time constants of the temperature and heat flux of the external fluid is significant, this difference being related to the thermal inertia of the external wall.

6. Conclusions

6.1. This article presents a comprehensive experimental study of a bitubular HEX considered as a lumped system with gas-gas flows, and subjected to various common transient conditions:
- quasi-stepped positive or negative variations in the temperature of the internal hot fluid,
- stepped positive or negative variations in the mass flow rate of the external cold fluid.

6.2. For both cases, the influence of the perturbation amplitude on various time constants was analyzed, as well as the influence of the mass flow rates of the two fluids, the inlet temperature of the hot fluid, and the HEX configuration (parallel-flow or counter-flow).

6.3. Experiments were conducted with gas-gas flows, compared to the main existing analytical model proposed in the literature and validated to date primarily with liquid-liquid flows.

6.4. The time lag (relaxation time) is negligible in the great majority of experiments. Generally, the non-ideality of the variation is accounted for by a short time constant τ_C (neglected here). Only the long-time constant τ_L is representative of the HEX thermal response. The intermediate parameters (T_1, P_1, DP_1 not shown here) of the two exponential fittings are necessary to adjust the experimental responses (second order) of the perturbed fluid.

6.5. The existence of different time constants for the exit temperature responses of the gas-gas HEX configuration is reported, in comparison with the single time constant associated with a liquid-liquid HEX configuration.

6.6. The same conclusion was reached for the heat flux responses (extensive responses) of the two gaseous fluids and compared to the differential thermal power, representative of the heat capacity of the HEX. The corresponding time constant is always intermediate between those of the two fluids.

6.7. The single time constant of the reference model is currently much lower than the experimental results obtained for the temperature response. The time constant of the non-perturbed fluid temperature is the closest to the previous theoretical value, particularly when the external flow rate is perturbed.

6.8. The time constants of the perturbed fluid are lower than those of the non-perturbed fluid.

A sensitivity analysis of the time constants to the main system parameters was performed. The main conclusions of this analysis are as follows:

6.9. Parallel- and counter-flow configurations implies only slight differences in the τ's values, with $\tau_{parallel\text{-}flow} > \tau_{counter\text{-}flow}$.

6.10. The amplitude ΔT_i does not significantly influence the time constants τ_i.

6.11. However, $\Delta\dot{V}_{ext}$, the variation in the flow rate of the external cold fluid, has a strong and differentiated influence on time constants. A significant dissymmetry is observed between the cases where $\Delta\dot{V}_{ext}$increases and decreases. This asymmetry could be primarily due to the thermal inertia of the external wall.

6.12. The mass flow rates of the two fluids have a considerable influence on the values of τ. It has been shown that as the mass flow rate of the internal fluid $\dot{m}_{int}$ increases, each τ_{int} decreases. The time constant τ_{int} associated with the fluid, that corresponds to the varying parameter, is the most affected.

6.13. Several new perspectives emerge from this work, as follows:

- ❖ A local experimental study within the HEX has been partially completed (results will be published soon).
- ❖ Extension to other fluid flow configurations (liquid-gas, gas-liquid, two phase flows) appears promising.
- ❖ The development of more complete and adapted models has been initiated, including:
  - an analytical diabatic model [53],
  - two phases flow model,
  - numerical models.

However, we wish to preserve simplicity and robustness of the models in order to successfully apply them to control and command of HEX (real time applications).

The experimental results and their detailed discussion allow, through the equivalence to bitubular configuration, to consider them in the control-oriented modeling of complex HEX network. In addition, the complexity of the presentation was intended to permit the use of the acquired knowledge regarding the influence of existing parameters in current and future experiments in HEX with phase change (liquid-liquid to vapor-vapor or vice-versa) or in transient systems, such as engines, cooler and heat pumps.

Author Contributions

M.F.: conceptualization, methodology, software, validation, writing—original draft preparation, supervision; M.C.: validation, formal analysis, writing—review and editing, visualization, supervision, project administration. All authors have read and agreed to the published version of the manuscript.

Institutional Review Board Statement

Not applicable.

Informed Consent Statement

Not applicable.

Data Availability Statement

All data are available near the authors.

Acknowledgments

The authors sincerely thank Cédric Jacquot for his help during the experimental work.

Conflicts of Interest

The authors declare no conflict of interest.

Use of AI and AI-Assisted Technologies

No AI tools were utilized for this paper.

Nomenclature

C_p	Specific heat at constant pressure (J kg^{-1}K^{-1})
DP	Differential heat flux (W)
DP_1	Transition differential heat flux (W)
$\dot{m}$	Mass flow rate (kg s^{-1})
P	Heat transfer rate or flux (W)
P_1	Transition heat flux (W)
Pr	Pressure (bar)
T	Temperature (°C)
T_1	Transition temperature (perturbed fluid) (°C)
t	Time (s)
t_r	Time lag (s)

$\dot{V}$	Volume flow rate at normal state condition (Nm^3h^{-1})
τ	Temperature time constant (s)
τ_P	Heat flux time constant (s)
τ_{DP}	Differential heat flux time constant (s)
ΔT	Temperature perturbation (°C)
$\Delta\dot{V}$	Volume flow rate perturbation at normal state condition (Nm^3h^{-1})
Subscript:	
amb	Ambiance
C	Short time (fluid perturbed)
e	Inlet
ext	External fluid
int	Internal fluid
L	Long time (fluid perturbed)
ref	Standard model (reference)
s	Outlet
Superscript:	
0	Initial state
∞	Final state
Abbreviation:	
CNES	National Center for Space Studies
ELX	CNES software
F.S.	full scale
HEX	Heat exchanger

References

1. Pierson, P. Etude Théorique et Expérimentale de Systèmes Thermiques en Régime Instationnaire : Échangeurs Capteurs Solaires et Installations Solaires Actives. Ph.D. Thesis, Université of Reims, Reims, France, 1986.
2. Feidt, M.; Costea, M.; Stanciu, C.; et al. *Génie Énergétique Appliqué au Solaire—Énergie Solaire Thermique*; Printech: Bucharest, Romania, 2004.
3. Ordonneau, G.; Albano, G.; Masse, J. CARINS: A future versatile and flexible tool for engine transient prediction. In Proceeding of the 4th International Conference on Launcher Technology "Space Launcher Liquid Propulsion", Liège, Belgium, 3–6 December 2002.
4. Feidt, M. Comportement en régime variable de machines thermiques à cycles inverses et de leurs composants. In *P.R.2.9., VARITHERM, Final Report*; A.C. Energy Colloqium, C.N.R.S.: Grenoble, France, 2005.
5. Pfafferott, T.; Schmitz, G. Modelling and transient simulation of CO_2 refrigeration system with Modelica. *Int. J. Refrig.* **2004**, *27*, 42–52. https://doi.org/10.1016/S0140-7007(03)00098-7.
6. Li, X.; Shu, G.; Tian, H.; et al. Experimental comparison of dynamic responses of CO_2 transcritical power cycle systems used for engine waste heat recovery. *Energy Convers. Manag.* **2018**, *161*, 254–265. https://doi.org/10.1016/j.enconman.2018.02.010.
7. Yang, R.; Tran, C.T. An analytical heat exchanger model to study dynamic behavior in the case of simultaneous inlet variations. *Int. J. Therm. Sci.* **2022**, *174*, 107452. https://doi.org/10.1016/j.ijthermalsci.2021.107452.
8. Kimiaei, S.; Kazemi-Ranjbar, S.; Jalali, A.; et al. A novel three-dimensional numerical model to simulate heat transfer inside a double U-tube borehole with two independent circuits. *Int. J. Heat Mass Transf.* **2022**, *184*, 122243. https://doi.org/10.1016/j.ijheatmasstransfer.2021.122243.
9. Romie, F.E. Transient response of crossflow heat exchangers with zero core thermal capacitance. *ASME J. Heat Transf.* **1994**, *116*, 775–777. https://doi.org/10.1115/1.2910939.
10. Fotowat, S.; Askar, S.; Fartaj, A. Experimental transient response of a minichannel heat exchanger with step flow variation. *Exp. Therm. Fluid Sci.* **2017**, *89*, 128–139. https://doi.org/10.1016/j.expthermflusci.2017.08.004.
11. Roberts, R.A.; Doty, J.H. Implementation of a transient exergy analysis for a plate-fin heat exchanger. *IJEX* **2015**, *16*, 109–126. https://doi.org/10.1504/IJEX.2015.067302.
12. Jedlikowski, A.; Anisimov, S.; Danielewicz, J.; et al. Frost formation and freeze protection with bypass for counter-flow recuperators. *Int. J. Heat Mass Transf.* **2017**, *108*, 585–613. https://doi.org/10.1016/j.ijheatmasstransfer.2016.12.047.
13. Nakashima, A.T.D.; Peixer, G.F.; Lozano, J.A.; et al. A lumped-element magnetic refrigerator model. *Appl. Therm. Eng.* **2022**, *204*, 117918. https://doi.org/10.1016/j.applthermaleng.2021.117918.
14. Ja'fari, M.; Jaworski, A.J.; Piccolo, A.; et al. Numerical study of transient characteristics of a standing-wave thermoacoustic heat engine. *Int. J. Heat Mass Transf.* **2022**, *186*, 122530. https://doi.org/10.1016/j.ijheatmasstransfer.2022.122530.
15. Ataer, O.E. An approximate method for transient behavior of finned-tube-cross flow heat exchangers. *Int. J. Refrig.* **2004**, *27*, 529–539. https://doi.org/10.1016/j.ijrefrig.2004.02.005.

16. Krishnakumar, K.; John, A.K.; Venkatarathnam, G. A review of transient test techniques heat transfer design data of compact heat exchanger surfaces. *Exp. Therm. Fluid Sci.* **2011**, *35*, 738–743. https://doi.org/10.1016/j.expthermflusci.2010.12.006.
17. Roetzel, W.; Xuan, Y. Transient response of parallel and counterflow heat exchangers. *ASME J. Heat Transf.* **1992**, *114*, 510–512. https://doi.org/10.1115/1.2911304.
18. Gao, T.Y.; Sammakia, B.; Geer, J.; et al. Transient effectiveness characteristics of cross flow heat exchangers in data center cooling systems. In Proceedings of the Fourteenth Intersociety Conference on Thermal and Thermomechanical Phenomena in Electronic Systems (ITherm), Orlando, FL, USA, 27–30 May 2014; pp. 688–697.
19. Su, F.; Prasad, R.C. A transient experimental method to determine the overall heat transfer coefficient in a concentric tube heat exchanger. *Int. Comm. Heat Mass Trans.* **2003**, *30*, 603–614. https://doi.org/10.1016/S0735-1933(03)00098-8.
20. Askar, S.; Fotowat, S.; Fartaj, A. Transient experimental investigation of airside heat transfer in a crossflow heat exchanger. *Appl. Therm. Eng.* **2021**, *199*, 117516. https://doi.org/10.1016/j.applthermaleng.2021.117516.
21. Gao, T.Y.; Sammakia, B.; Geer, J. Dynamic response and control analysis of cross flow heat exchangers under variable temperature and flow rate conditions. *Int. J. Heat Mass Transf.* **2015**, *81*, 542–553. https://doi.org/10.1016/j.ijheatmasstransfer.2014.10.046.
22. Gao, T.Y.; Geer, J.; Sammakia, B. Review and analysis of cross flow heat exchanger transient modeling for flow rate and temperature variations. *J. Therm. Sci. Eng. Appl.* **2015**, *7*, 041017. https://doi.org/10.1115/1.4031222.
23. Bobic, M.; Gjerek, B.; Golobic, I.; et al. Dynamic behaviour of a plate heat exchanger: Influence of temperature disturbances and flow configurations. *Int. J. Heat Mass Transf.* **2020**, *163*, 120439. https://doi.org/10.1016/j.ijheatmasstransfer.2020.120439.
24. Romie, F.E. Transient response of the counter flow heat exchanger. *ASME J. Heat Transf.* **1984**, *106*, 620–626. https://doi.org/10.1115/1.3246725.
25. Lahzazi, A.; Galanis, N. Thermal transients in parallel flow heat exchangers. In Proceedings of the International Symposium on Transient Convective Heat and Mass Transfer in Single and Two-phase Flow, Cesme, Turkey, 17–22 August 2003; pp. 333–342.
26. Henrion, M.; Feidt, M. Comportement en régime transitoire de divers types d'échangeurs de chaleur ; Modélisation et conséquences. *Int. Commun. Heat Mass Trans.* **1991**, *18*, 731–740. https://doi.org/10.1016/0735-1933(91)90084-H.
27. Pierson, P.; Padet, J. Etude théorique et expérimentale des échangeurs en régime thermique instationnaire. Simulation d'une phase de relaxation. *Int. J. Heat Mass Transf.* **1988**, *31*, 1577–1586. https://doi.org/10.1016/0017-9310(88)90270-0.
28. Pierson, P.; Azilinon, D.; Padet, J. Simulation du fonctionnement des échangeurs thermiques soumis à des conditions aux limites variables. *Rev. Phys. Appl.* **1989**, *24*, 93–107. https://doi.org/10.1051/rphysap:0198900240109300.
29. Hadidi, M.; Guellal, M.; Lachi, M.; et al. Loi de réponse d'un échangeur thermique soumis à des échelons de température aux entrées. *Int. Commun. Heat Mass Trans.* **1995**, *22*, 145–154. https://doi.org/10.1016/0735-1933(94)00060-X.
30. Azilinon, D.; Pierson, P.; Padet, J. Constante de temps des échangeurs thermiques. *Rev. Gen. Therm.* **1990**, *338*, 64–78.
31. Lachi, M.; Elwakil, M.; Padet, J. The time constant of double pipe and one pass shell and tube HEX in the case of varying fluid flow rates. *Int. J. Heat Mass Transf.* **1997**, *40*, 2067–2079. https://doi.org/10.1016/S0017-9310(96)00274-8.
32. Abdelghani-Idrissi, M.-A.; Bagui, F.; Estel, L. Countercurrent Double-Pipe Heat Exchanger Subjected to Flow-Rate Step Change, Part II: Analytical and Experimental Transient Response. *Heat Transf. Eng.* **2002**, *23*, 12–24. https://doi.org/10.1080/01457630290090617.
33. Abdelghani-Idrissi, M.A.; Bagui, F.; Estel, L. Analytical and experimental response time to flow rate step along a counter flow double pipe HEX. *Int. J. Heat Mass Transf.* **2001**, *44*, 3721–3730. https://doi.org/10.1016/S0017-9310(01)00023-0.
34. Balbi, J.H.; Balbi, N.; Orenga, P.; et al. Modélisation du champ de capteurs de la centrale solaire de Vignola. *Rev. Phys. Appl.* **1986**, *21*, 169–180. https://doi.org/10.1051/rphysap:01986002102016900.
35. Aboudi, S.; Papini, F. Etude numérique du transfert thermique métal-fluide dans un conduit rectangulaire en régime instationnaire. *Int. J. Heat Mass Transf.* **1990**, *33*, 1909–1920. https://doi.org/10.1016/0017-9310(90)90222-G.
36. Siakavellas, N.J.; Georgiou, D.P. 1D heat transfer through a flat plate submitted to step changes in heat transfer coefficient. *Int. J. Therm. Sci.* **2005**, *44*, 452–464. https://doi.org/10.1016/j.ijthermalsci.2005.01.003.
37. Dwivedi, A.K.; Das, S.K. Dynamics of plate heat exchangers subject to flow variations. *Int. J. Heat Mass Transf.* **2007**, *50*, 2733–2743. https://doi.org/10.1016/j.ijheatmasstransfer.2006.11.029.
38. Romie, F.E. Response of counterflow heat exchangers to step changes of flow rates. *ASME J. Heat Transf.* **1999**, *121*, 746–748. https://doi.org/10.1115/1.2826046.
39. Fotowat, S.; Askar, S.; Fartaj, A. Transient response of a meso heat exchanger with temperature step variation. *Int. J. Heat Mass Transf.* **2018**, *122*, 1172–1181. https://doi.org/10.1016/j.ijheatmasstransfer.2017.12.062.
40. Mishra, M.; Das, P.K.; Sarangi, S. Transient behaviour of crossflow heat exchangers due to perturbations in temperature and flow. *Int. J. Heat Mass Transf.* **2006**, *49*, 1083–1089. https://doi.org/10.1016/j.ijheatmasstransfer.2005.09.003.
41. Singh, S.K.; Mishra, M.; Jha, P.K. Transient behaviour of co-current parallel flow three-fluid heat exchanger. *Int. Comm. Heat Mass Trans.* **2014**, *52*, 46–50. https://doi.org/10.1016/j.icheatmasstransfer.2014.01.001.

42. Jacquot, C. Transfert Instationnaire de Chaleur en Échangeur Récupérateur de Moteur de Fusée; Simulation Expérimentale et Théorique en Échangeur Bitube. Ph.D. Thesis, Université Henri Poincaré, Nancy, France, February 2007.
43. Roetzel, W.; Das, S.K.; Luo, X. Measurement of heat transfer coefficient in plate HEX using a temperature oscillation technique. *Int. J. Heat Mass Transf.* **1994**, *37*, 325–331. https://doi.org/10.1016/0017-9310(94)90033-7.
44. Petit, D.; Dard, J.; Degiovanni, A. Détermination du coefficient d'échange entre un fluide et une paroi. *Rev. Gen. Therm.* **1981**, *20*, 719–732.
45. Rebay, M.; Lachi, M.; Padet, J. Mesure du coefficient de convection par méthode impulsionnelle—Influence de la perturbation de la couche limite. *Int. J. Therm. Sci.* **2002**, *41*, 1161–1175. https://doi.org/10.1016/S1290-0729(02)01402-3.
46. Luo, X.; Roetzel, W. The single-blow transient technique for plate-fin heat exchangers. *Int. J. Heat Mass Transf.* **2001**, *44*, 3745–3753. https://doi.org/10.1016/S0017-9310(01)00019-9.
47. Froilabo. Available online: www.froilabo.com (accessed on 21 February 2026).
48. Air Liquide. *Encyclopédie des Gaz*; Elsevier: Amsterdam, The Netherlands, 1976.
49. TCSA. Available online: www.tcsa.fr (accessed on 24 March 2026).
50. Instrutec. Available online: www.instrutec.fr (accessed on 21 February 2026).
51. SAIS. Available online: www.sais.fr (accessed on 24 March 2026).
52. Moffat, R.J. Describing the uncertainties in experimental results. *Exp. Therm. Fluid Sci.* **1988**, *1*, 3–17. https://doi.org/10.1016/0894-1777(88)90043-X.
53. Jacquot, C.; Feidt, M.; Corvisier, P.; et al. Transient convective heat and mass transfer in diabatic heat exchangers: Application to cryogenic heat exchangers. In Proceedings of the International Symposium on Transient Convective Heat and Mass Transfer in Single and Two-phase Flow, Cesme, Turkey, 17–22 August 2003; pp. 323–332.